Neuron, Volume *58*

# High frequency organization and synchrony of activity in the Purkinje cell layer of the cerebellum

C. de Solages et al.

## Supplementary information

Contents :

# Supplementary Figures

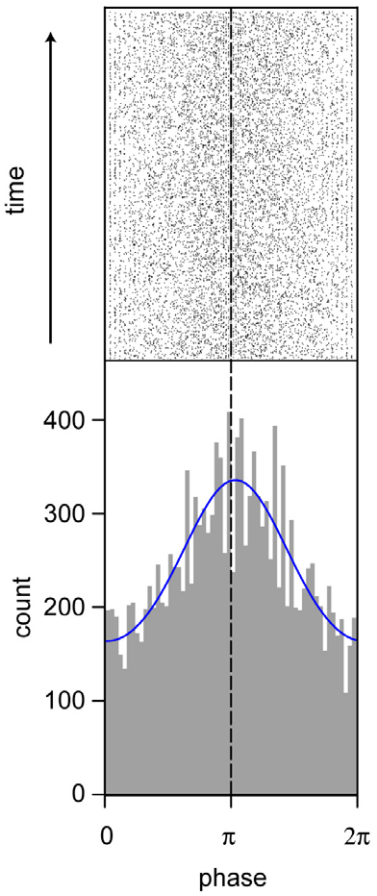


**Figure 1 :** Activity in the Purkinje cell layer is phase-locked to high frequency oscillations

Legend :

Example of phase locking to the high frequency oscillations of spiking activity in the Purkinje cell layer. top : raster of the spike train phases, bottom : corresponding phase value distribution with a von Mises fit.

Methods and results :

In 6 experiments with linear probes of 16 electrodes, with the probe perpendicular to the surface of the lobule, extracellular potential were recorded simultaneously in the 3 layers of the cerebellar cortex (see Methods). It has been shown (see Results and fig. 4) that oscillations are in phase in the Purkinje cell layer, where the spiking activity is intense, and in

the granule cell layer, where the spiking activity is undetectable. We therefore studied the phase relation between spikes in the Purkinje cell layer and oscillations in the granule cell layer. Analysis was performed on 1min-long recordings. Spikes were extracted from the channel recorded in the Purkinje cell layer : continuous recordings were high-pass filtered at 600Hz (with a Butterworth filter) before thresholding at 3 times the standard deviation of filtered signal. Oscillation peaks were extracted from a channel in the granule cell layer, in which no spikes were present: continuous recordings were band-pass filtered between 100 and 250Hz and peaks were extracted. The distance between the 2 recordings sites varied from 100 to 250μm.

For each case, the significance of phase locking was evaluated by applying the Rayleigh test for circular uniformity on the phase value distribution. In 6/6 cases, spikes were significantly phase-locked (all p-values were inferior to $10^{-20)}$. For each case, phase distribution was fitted with a von Mises distribution. The von Mises distribution is the circular analog of the normal distribution and is parameterized by a mean direction μ, and a concentration parameter κ, with larger values corresponding to more peaked distributions. The mean of the maximum likelihood estimates for the von Mises mean direction parameters was 198.3° +/- 10.09° (mean+/-s.d.). The mean concentration parameter κ was 0.24 +/- 0.06 (mean+/-s.d.). The population activity in the Purkinje cell layer therefore has a preferred phase on the troughs of the oscillation but the concentration of the phase distribution isn't very high indicating partial phase-locking.

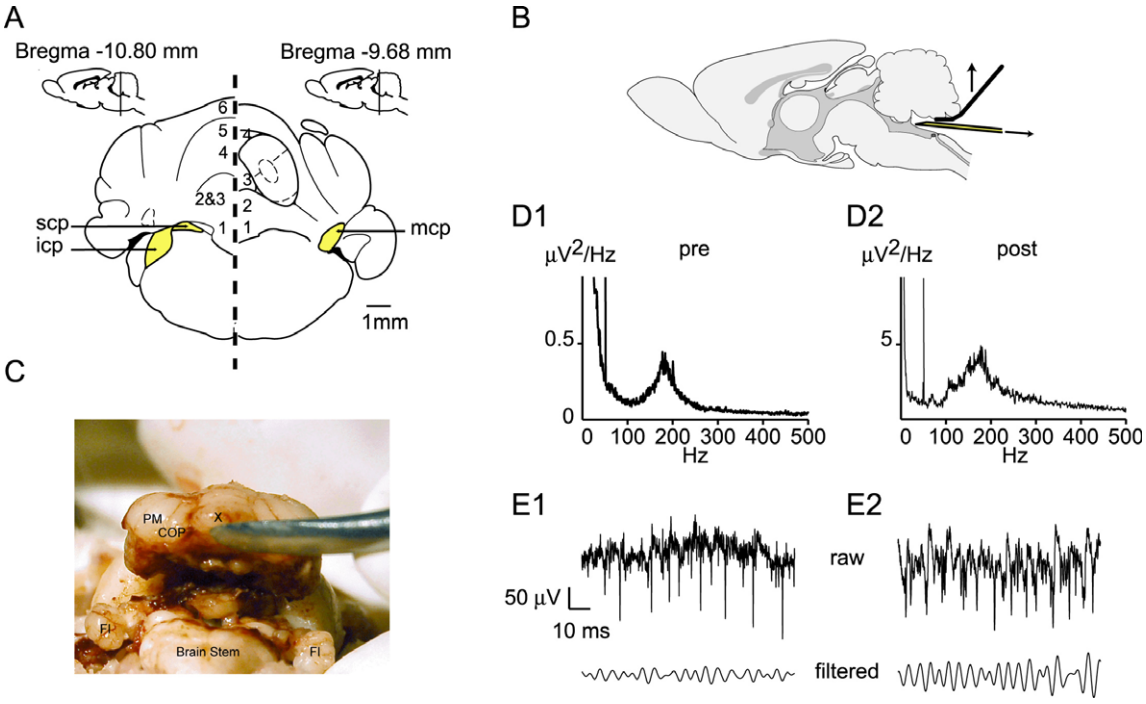


**Figure 2** : High-frequency oscillations are present after the cerebellum as been disconnected from the rest of the brain by pedunculectomy

Legend :

**(A)** Diagram of transverse views of the rat brain showing the localization of the cerebellar peduncles (scp, icp, mcp = respectively superior, inferior and median cerebellar peduncles). The number corresponds to the cerebellar lobules visible on the scheme. **(B)** Principle of the pedunculectomy shown on a sagittal scheme of rat brain. **(C)** Picture of the pedunculectomized cerebellum after fixation. The cerebellum has been lifted to evidence the separation from the brain stem. X=cerebellar lobule 10, PM= paramedian lobule, COP=copula, FL=floculus. **(D)** Example of spectra of local field potential before (D1) and after (D2) pedunculectomy. **(E)** Example of recorded signal before (E1) and after (E2) pedunculectomy. up = raw signal, low =120-250Hz band-pass filtered signal

Methods and results :

The three cerebellar peduncles were cut on each side using a posterior approach. Vermis and hemispheres were uncovered removing posterior and superior bones. Then, from the fourth ventricle, the cerebellum was gently pushed upwards to expose the posterior peduncles. They were manually cut under a surgical microscope, using a blunt needle connected to suction.

At the end of the recording sessions, a dose of pentobarbital (30mg/kg i.p.) was added, the animal trans-cardiacally rinsed with ringer, perfused with formalin and the head kept overnight in formalin. Peduncular sections were checked by careful examination.

Full pedunculectomy was obtained in three rats and fast oscillations were visible in the different layers of the cerebellar cortex of these animals.

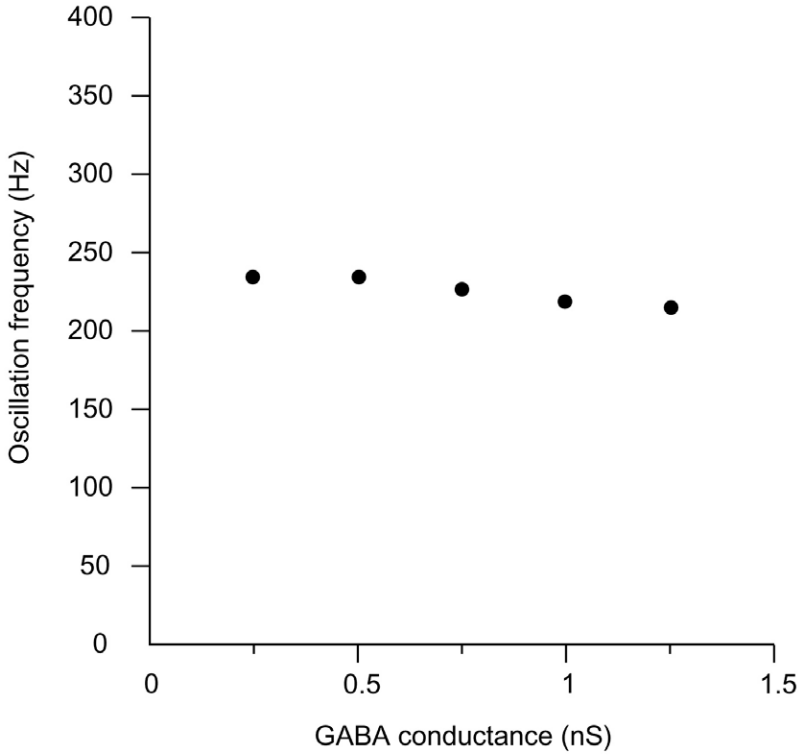


**Figure 3 :** The population oscillation frequency is not sensitive to the strength of the recurrent inhibitory conductance

Legend :

Network frequency as a function of synaptic conductance.

Methods :

The model used for the simulation is the one described in the Methods section. The synaptic conductance was varied between 0.25 and 1.25nS while keeping the other parameters fixed at their reference value (latency=1.5ms, rise time=0.5ms, decay time=3ms, s=100pA) .

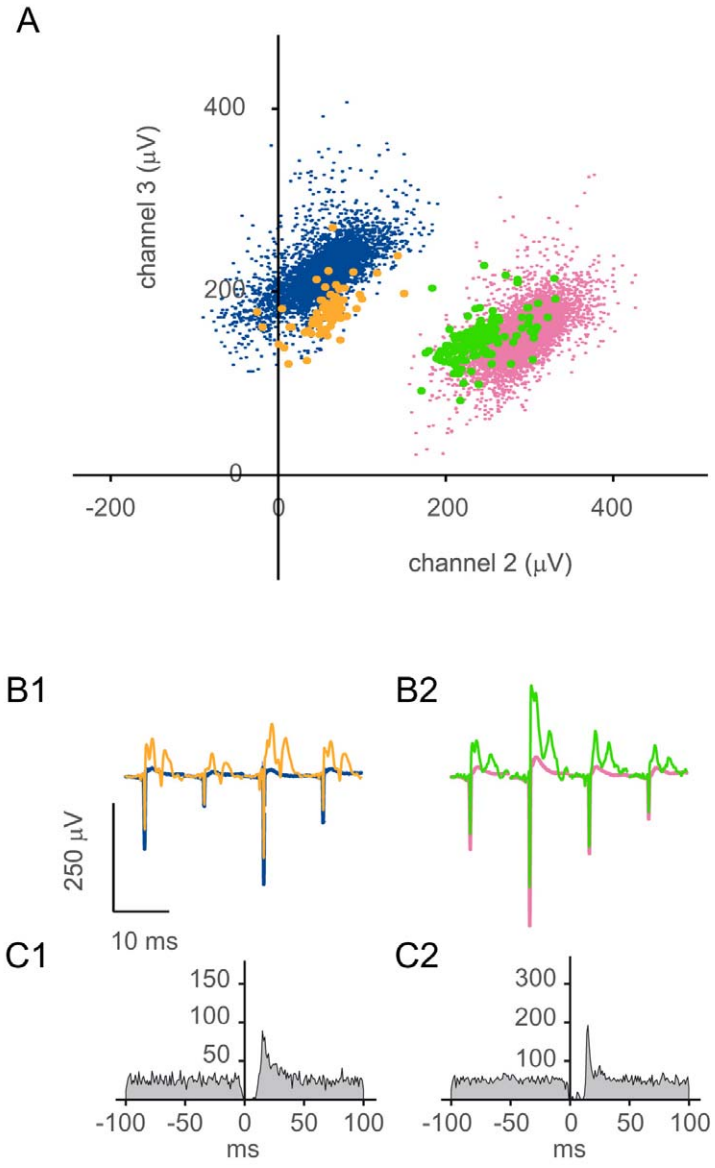


**Figure 4 :** Complex spikes and simple spikes have the same ratios of amplitudes on the 4 channels

Same example as figure 1 in the manuscript. Complex spikes were isolated for units 1 and 4 of the example. Simple spikes are in blue and pink respectively. Complex spikes are in orange and green respectively. **(A)** Plot of sorted spikes of the two units on two channels of the tetrode. Same projection as in Fig.1. (The spikes of other units and unassigned spikes are not displayed). **(B)** Average unfiltered waveforms on the four tetrode channels. Simple and complex average spikes are superimposed to show the conservation of amplitude ratio over the four channels of the initial spike of the complex spike with that of the simple spike.(B1)

and (B2) correspond to units 1 and 4 respectively. Same colors as in (A). **(C)** The cross-correlogram between complex and simple spikes show the pause of simple firing after the emission of a simple spike. (C1) and (C2) correspond to units 1 and 4 respectively.

# Supplementary Methods

## Quantification of cross-correlograms

To compute the significance in cross-correlation analysis, we used the standardized cross-covariance (Siapas et al. 2005). The cross-covariance was derived from the cross-correlation histogram $J_{12}^{T,b}(u)$ of the units 1 and 2, which counts the number of spike pairs (i,j) of the units 1 and 2 occurring at times $(t_1(i),t_2(j))$ such that $|t_1(i)-t_2(j)-u| < b/2$, with b being the bin size. The standardized cross-covariance was taken as $Q_{12}(u)= (J_{12}^{T,b}(u)-A)/ \text{sqrt}(A)$, with $A=N_1.N_2.b/T$, with $N_1$ and $N_2$ being the total number of spikes recorded from the units 1 and 2, and T being the recording duration. For independent spike trains, the asymptotic distribution of the standardized cross-covariance is approximately normal $Q_{12}(u) \sim N(m=0, s^2=1)$, and therefore spike-train independence was not verified when $|Q_{12}(u)|>z_{crit}$. For a +/-30 ms cross-correlation histogram, the hypothesis of spike train independence could be rejected for any of the 60 time-lags. The level of significance ($p<0.05$) was thus divided by 60 yielding a critical z-value of 3.34.

## Spectral analysis

Spectral density estimates were obtained with Welch's method with windows of $2^{15}$ points (1.3ms at 25kHz) for continuous signals or $2^9$ points (0.5s at 1kHz) for spike trains. The spike train spectral analysis was performed using a 1kHz synthetic signal whose value at time $t_i$ corresponds to the number of spikes falling in the 1ms interval $t_i$-$t_{i+1}$. The peaks in the spectrum of single units were usually narrow enough to be localized by taking the position of the absolute maximum in the spectrum. To analyze the high-frequency organization in multi-unit spike trains, the synthetic spike trains from each unit were summed to form a synthetic multi-unit signal, whose spectral density was computed. To remove the contribution of single unit spectra to this multi-unit spectrum, we subtracted from it a shuffled spectrum obtained from a multi-unit signal generated by the summation of independently time-shifted single-unit spike trains (This operation was not performed for the spectrum displayed in Figure 3C). Since the temporal coordination between the spike trains was disrupted by the introduction of the time shifts, this shuffled multi-unit spectrum only reflected the spectral characteristics of

multiple independent single units. The characteristics of peaks in multi-unit spectra were obtained by fitting the spectrum with a Lorentzian curve in the frequency range of interest (100-350Hz). The peak frequencies in extracellular potential spectra were obtained from a fit of the power spectrum with a Lorentzian curve (chosen simply because of its appropriate shape) added to a linear trend. For pharmacological studies, the spectra from the four channels of the tetrode were averaged before performing the fit.

***In vitro* electrophysiology:**

Procedures to protect adult tissue during slice preparation were adapted from (Isope and Barbour 2002). Briefly, adult male Wistar rats (2-4 months old) were anesthetized with ketamine/xylazine (75 and 10mg/kg, respectively) intraperitoneally. Then pentobarbital doses (20mg/kg) were administered if required to ensure attainment of the surgical plane of anesthesia (total abolition of plantar withdrawal reflex to nocive stimuli). Transcardiac perfusion of the rat with two cold, bubbled (95%O2/5%CO2) solutions was established. Solution 1 (150ml) contained (in mM): 115 NaCl; 26 NaHCO3; 3 KCl; 0.8 CaCl2; 8 MgCl2; 1.25 NaH2PO4; 25 D-glucose; 1 lidocaine-HCl; 1 ketamine-HCl. Solution 2 (100ml) was identical except that sucrose (230mM) replaced the NaCl. As soon as perfusion was under way, the abdominal aorta and/or the inferior vena cava were/was clamped. After perfusion the rat was decapitated. Care was taken to avoid unnecessary cutting or deforming the cerebellum during dissection. The cerebellum was cooled and sliced in solution 2 supplemented with 50μM D-APV.

Sagittal slices 360-450μm thick were cut using a Microm HM650V slicer. Slices recovered for 60min in standard extracellular saline at 33°C, containing (in mM): NaCl 125; $NaHCO_3$ 26, KCl 3; $NaH_2PO_4$ 1.25, $CaCl_2$ 2; $MgCl_2$ 2; D-glucose 25; bubbled with 95%$CO_2$/5%$O_2$. Thereafter, the slices were stored at room temperature. Whole-cell voltage-clamp recordings were obtained at 31–32°C from Purkinje cells using a Cairn Optopatch. Cells were usually clamped to –65mV, and series resistance was compensated (50-70% of 5-12MΩ, typically) as appropriate. A CsCl-based internal solution was used. The composition of this solution was (in mM): CsCl 125; QX-314 Cl-1; HEPES 10; $MgCl_2$ 1; $CaCl_2$ 0.5; TEA-Cl 10; BAPTA 10; $Na_2ATP$ 4; NaGTP 1; titrated to pH 7.3 with CsOH.

Recordings were carried out in a solution containing (in mM): NaCl 125; $NaHCO_3$ 26, KCl 3; $NaH_2PO_4$ 1.25, $CaCl_2$ 2; $MgCl_2$ 2; D-glucose 25; bubbled with 95 %$CO_2$/5 %$O_2$. 2,3-Dioxo-6-nitro-1,2,3,4-tetrahydrobenzo[f]quinoxaline-7-sulfonamide disodium salt (NBQX) 10µM was present in the solution unless specified. WIN 55,212-2 (WIN) and AM 251 were used at 5µM (diluted from a 5mM stock in DMSO). Chemicals and drugs were obtained from Sigma and Tocris. All solutions lines were washed with ethanol 90% (300ml) and water (1L) between recordings to remove WIN and AM 251.

To evoke IPSCs, minimal electrical stimulations were performed with a patch pipette filled with extracellular solution and 200µs electrical voltage steps of 10-30V. The GABAergic nature of spontaneous and evoked IPSCs was verified by bicuculline application (10µM, n=2). The kinetics of the IPSCs were fitted with the difference of two exponentials, whose time constants provide the rise time and decay values, and employed in the model. In one experiment, a population of large spontaneous IPSCs appeared after the application of WIN corresponding to a 475% increase in the average IPSCs amplitude; this experiment was not included in the analysis. To study evoked EPSCs, minimal electrical stimulations in the granule cell layer were performed in the presence of picrotoxin 10µM and in the absence of NBQX.

**Experiments in the unanesthetized animal**

The animals underwent surgery under isoflurane. An antiseptic ointment was applied to the wound around the pedestal and an antibiotic (cefuroxime, 60mg/kg i.p.) was administered during 7 days after the surgery.

For freely-moving rat, a home-made multi-tetrode implant was placed over the cerebellar hemisphere.

For pharmacological experiments in the head-restraint animal, a pedestal of dental acrylic cement including three screws was built to allow atraumatic fixation of the animal head during subsequent recording sessions. The bone was removed and a recording chamber was placed over the cerebellar vermis. The chamber was hermetically closed with a silicon elastomeric impression material (Provil Novo monophase, Hereaeus Kulzer, Germany). A

screw was fixed to the skull to be used as recording ground. The animals were adapted to restrained conditions 2 days after surgery. The animal was placed in a loose bag with the head fixed for increasing periods of time (from a few minutes to 2 hours; this duration was shortened whenever animals exhibited discomfort). The animal received sweetened condensed milk as a reward at the end of the restraint. At the end of the period of adaptation (5-6 days), the animal was anesthetized to remove the dura mater above the cerebellar vermis. Daily recording sessions (1-2h) were then performed. No more than 2 different recording sites belonging to distinct Purkinje cell layers were considered for each animal on a given day. A pipette was glued to the holder of the tetrode in order to minimize the distance between the two tips (<200mm, Figure 10B). The pipette was connected to a pressure ejection system. When a recording site was chosen, the drug was ejected by pulses of 0.3 to 2.8 bars lasting 15s to several minutes. The level of the liquid in the pipette was monitored visually to confirm the ejection and to adjust the pressure. WIN 55,212-2 (1mg/mL) was dissolved in 1mL vehicle containing 0.98ml saline, 20ml DMSO and 450mg Hydroxypropyl-b-cyclodextrin.

The recordings were performed with tetrodes in the Purkinje cell layer as in the anesthetized animal. The Purkinje cell layer was approached from the molecular layer. The tetrode was adjusted at the frontier between the Purkinje cell layer and the molecular layer so that the tip was in the Purkinje cell layer and at least one of the other channels remained in the molecular layer; this configuration allowed us to verify that no tetrode movement occurred during the recording.

## References

Sapias, A.G., Lubenov, E.V., Wilson, M.A. (2005). Prefrontal phase locking to hippocampal theta oscillations. Neuron *46*, 141-51.

Isope P., Barbour B. (2002). Properties of unitary granule cell-->Purkinje cell synapses in adult rat cerebellar slices. J. Neurosci *22*, 9668-78.

# Supplementary information for the model

The model network was composed of 200 neurons, with a connection probability of 20% estimated from the extension of reconstructed Purkinje cell axons (Bishop and O'Donoghue, 1986). Each Purkinje cell was modelled as a two-compartment leaky integrate-and-fire neuron, whose parameters were based on fitting adult Purkinje cell current responses to voltage jumps (Barbour, unpublished). This fitting procedure gave: Csoma=30pF, Cdendrite=1500pF, gsoma=0.6nS, gdendrite=60nS, gsd(soma to dendrite axial conductance)=270nS. The soma had therefore short time constant in response to current injection (0.1ms, corresponding to Csoma/(gsoma*gsd)). The threshold for firing of the somatic compartment was set to -50mV and, following a spike, the soma was reset to -60mV after a 2ms refractory period. GABAergic connections between cells were modelled as inhibitory conductances on the soma, with a peak conductance of 0.75nS and a reversal potential of -70mV. The time course of the IPSC was described as a delayed difference of exponentials, with latency 1.5ms, rise time 0.5ms, and decay time 3ms, consistent with the *in vitro* electrophysiological observations. In addition, each cell received a depolarizing current which was drawn randomly and independently for each cell. Both mean and SD of these currents were chosen to reproduce the distribution of firing rates seen experimentally. This gave a mean current of 7.2 (720) nA in the soma (dendrite), with a SD of 20% around the mean. Finally, excitatory and inhibitory inputs from granule cells and interneurons were modelled as a stochastic current in the dendrite, which we chose to describe by an Ornstein-Uhlenbeck random process (Destexhe et al. 2001), with SD 500pA and correlation time constant 5ms. When the SD of the noise was changed, we adjusted the mean currents so that the mean single unit frequency remained unchanged. When rise and decay time constants were changed, we adjusted the amplitude of the synaptic conductance so that the total charge was unchanged. This led to a mean single cell frequency approximately independent of those parameters. A more detailed description of the model is provided below.

## Full description of the model

We simulated a network of N = 200 two-compartment leaky integrate-and-fire neurons. Neurons are connected randomly with 20% connection probability. Neuron i (i = 1, . . . ,N) is described by the membrane potential of both its soma $V_{s,i}$ and dendrite $V_{d,i}$ whose dynamics obey to the equations

$$C_{soma}\frac{dV_{s,i}(t)}{dt} = -g_{soma}(V_{s,i}(t)-V_i) - g_{sd}(V_{s,i}-V_{d,i}) - I_{i,GABA}(t) \quad (1)$$

$$C_{dendrite}\frac{dV_{d,i}(t)}{dt} = -g_{dendrite}(V_{d,i}(t)-V_i) - g_{sd}(V_{d,i}-V_{s,i}) - I_{i,noise}(t) \quad (2)$$

where $C_{soma}$ = 30 pF, $C_{dendrite}$ = 1500 pF, $g_{soma}$ = 0.6 nS, $g_{dendrite}$ = 60 nS, $g_{sd}$ = 270 nS, Vi is drawn randomly and independently from neuron to neuron using a Gaussian distribution with average −48 mV and SD 2.4 mV, in order to reproduce the distribution of firing rates seen in experiment.

$I_{i,GABA}(t)$ are GABAergic currents on the soma, described as

$$I_{i,GABA}(t) = (V_{s,i}(t)-V_I)g_I\sum_{j,k} s(t-t_j^k)$$

where $V_I$ = −70 mV, $g_I$ = 0.75 nS is the peak conductance of a single GABAergic synapse, and the adimentional variable $s(t - t^k_j)$ describes the time course of the conductance change induced by spike k of presynaptic neuron j occurring at time $t^k_j$. The sum runs over all presynaptic neurons that project to neuron i. s(t) is a delayed difference of exponentials, with a latency $\tau_L$ = 1.5 ms, a rise time $\tau_R$ = 0.5 ms, and a decay time $\tau_D$ = 3 ms. Such a time course is obtained from the following equations:

$$\frac{ds}{dt} = -\frac{s-\alpha x}{\tau_D} \quad (3)$$

$$\frac{dx}{dt} = -\frac{x}{\tau_R} + \delta(t-\tau_L) \quad (4)$$

where the normalization $\alpha = (\tau_D/\tau_R)^{\tau D/(\tau D-\tau R)}$ is chosen such that s peaks at a value of 1.

The stochastic currents on the dendrite are described by Ornstein-Uhlenbeck processes,

$$\tau_N\frac{dI_{i,noise}}{dt} = -I_{noise} + \sigma\sqrt{\tau_N}\eta_i(t) \quad (5)$$

where $\tau_N$ = 5 ms is the correlation time constant, σ = 500 pA is the amplitude of the fluctuations, and $\eta_i$ are uncorrelated Gaussian white noises with unit variance density. For this value of σ, the inter-spike interval (ISI) distribution of single neurons is qualitatively similar to the ISI distributions observed in experiment.

## Approximate analytical estimate of network frequency

Analytical studies of fast oscillations in networks of inhibitory neurons (Brunel and Hakim 1999; Brunel and Wang 2003) have shown that close to the onset of network oscillations, the network frequency f obeys the equation

$$\Phi_S(f) + \Phi_N(f) = \pi \qquad (6)$$

where $\Phi_S(f)$ is the phase shift of post-synaptic currents with respect to the presynaptic instantaneous firing rate, while $\Phi_N(f)$ is the phase shift of the modulated instantaneous firing rate of a neuron with respect to an oscillatory input. For synapses described by a delayed difference of exponentials,

$$\Phi_S(f) = 2\pi f \tau_L + \mathrm{atan}(2\pi f \tau_R) + \mathrm{atan}(2\pi f \tau_D)$$

The neuronal phase shift is in general much more complicated to evaluate analytically, though it is straightforward to obtain it numerically. In the simple case of integrate-and-fire neurons with temporally correlated noise of large amplitude, the neuronal phase shift is close to zero at any frequency (Brunel et al. 2001; Fourcaud and Brunel 2002) If the single neuron phase shift is close to zero, the network oscillation frequency can be estimated by setting $\Phi_N = 0$ in Eq. (6) (Brunel and Wang 2003). Interestingly, the network of two-compartment neurons has a frequency that is larger than this prediction, indicating a phase advance of single neurons at high frequencies.

## References


Bishop, G. A. and O'Donoghue, D. L. (1986). Heterogeneity in the pattern of distribution of the axonal collaterals of Purkinje cells in zone b of the cat's vermis: an intracellular HRP study. J. Comp. Neurol. *253*, 483-99.

Destexhe, A., Rudolph, M., Fellous, J.M. and Sejnowski, T.J. (2001). Fluctuating synaptic conductances recreate in vivo-like activity in neocortical neurons. Neuroscience *107*, 13-24.

Brunel, N., F. Chance, N. Fourcaud, and L. Abbott (2001). Effects of synaptic noise and filtering on the frequency response of spiking neurons. Phys. Rev. Lett. 86, 2186–2189.

Brunel, N. and V. Hakim (1999). Fast global oscillations in networks of integrate-and-fire neurons with low firing rates. Neural Comp. 11, 1621– 1671.

Brunel, N. and X.-J. Wang (2003). What determines the frequency of fast network oscillations with irregular neural discharges? J. Neurophysiol. 90, 415–430.

Fourcaud, N. and N. Brunel (2002). Dynamics of firing probability of noisy integrate-and-fire neurons. Neural Computation 14, 2057–2110.